

A CLOSE LOOK AT THE STATE TRANSITIONS OF GALACTIC BLACK HOLE TRANSIENTS DURING OUTBURST DECAY

E. KALEMCI¹, J. A. TOMSICK², R. E. ROTHSCHILD², K. POTTSCHMIDT^{3,4}, P. KAARET⁵

Draft version September 13, 2018

ABSTRACT

We characterize the evolution of spectral and temporal properties of several Galactic black hole transients during outburst decay using the data from well sampled PCA/RXTE observations close to the transition to the low/hard state. We find several global patterns of evolution for spectral and temporal parameters before, during, and after the transition. We show that the changes in temporal properties (sudden increase or decrease in the rms amplitude of variability) are much sharper than the changes in the spectral properties, and it is much easier to identify a state transition with the temporal properties. The spectral index shows a drop 3-5 days before the transition for some of our sources. The ratio of the power-law flux to the total flux in the 3-25 keV band increases close to the transition, which may mean that the system must be dominated by the coronal emission for the transition to occur. We also show that the power-law flux shows a sharp change along with the temporal properties during the transitions which may indicate a threshold transition volume for the corona. The evolution of the spectral and temporal properties after the transition is consistent with the idea that the inner accretion disk moves away from the black hole. Based on the evolution of spectral and temporal parameters and changes during the transitions, we discuss possible scenarios of how the transition is happening.

Subject headings: black hole physics – X-rays:stars

1. INTRODUCTION

X-ray observations of Galactic black holes (GBH) indicate that they are found in several distinct spectral states (Tanaka & Lewin, 1995; McClintock & Remillard, 2003). These states are generally determined by the relative strength of two different emission components: soft blackbody-like radiation from an optically thick, geometrically thin accretion disk and a harder component showing a power-law spectrum believed to originate from Compton upscattering of soft seed photons from the disk by a hot electron corona. Often a relation between the X-ray luminosity of the source and spectral states also exists. When the soft component dominates the spectrum, the 2–10 keV luminosity is relatively high ($\gtrsim 10^{37}$ ergs/s), and therefore this state is called the “high/soft state” (HS). When the hard component dominates, then usually the 2–10 keV luminosity is low ($\lesssim 10^{37}$ ergs/s), and this state is called the “low/hard state” (LS). This dependence shows that the mass accretion rate plays an important role in determining the spectral states. These states also differ in terms of their short-term timing properties. The HS is often characterized by lack of or a very low level of variability, whereas the LS shows very strong variability ($\sim 30\%$ rms in 0.04–4 Hz). Recently, changes in the radio properties are also associated with the spectral states. In the LS, compact, optically thick jets are observed (Fender et al., 2001). During state transitions optically thin outflows are detected (Corbel et al., 2001), and during the HS the radio emission is quenched (Fender et al., 2001). There are also cases for which both spectral components are present at comparable strength, characterized by parameters that are intermediate between those of the HS and the LS. For such a case, if the source flux is lower than the HS flux, the state is often called the “intermediate state” (IS), and if the flux is higher than the HS flux, it is called the “very high state” (VHS). We note that the classification of these states is not rigorously defined and is still an active topic of debate.

Most of the GBHs are observed during outbursts caused by a sudden, dramatic increase of mass accretion rate onto the black hole. Fig. 1 shows several examples of outburst light curves discussed in this report (see Kalemci 2002 for all of

the ASM light curves.). Because of the dependence of spectral states on the mass accretion rate, a GBH transient often follows a specific sequence of spectral states. It is usually observed in the LS at the beginning of the outburst. As flux increases, it makes a transition to the HS or the VHS. As the source decays towards quiescence, a transition to the LS is usually observed. Some transients might follow a more complicated sequence of states, and some stay in the LS throughout the outburst. It is generally believed that the state transitions involve large restructuring of the accretion geometry of GBHs (Esin, McClintock & Narayan, 1997; Zdziarski et al., 2002). Therefore, analysis of these sources during state transitions may probe the dynamics of their accretion structure. Although the mass accretion rate is a very important parameter determining the spectral states, it is unlikely that the states and transitions are solely determined by this parameter. Some sources show hysteresis of the transition luminosities (the luminosity of transition from LS to HS during the beginning of the outburst is much higher than the luminosity of the transition from HS to LS during the outburst decay, Miyamoto et al., 1995; Nowak, 2002), and for some sources, a second, independent parameter seems to be required to explain the complexity of transitions. It is not clear what this second parameter is. It can be the position of the inner edge of the accretion disk, but this parameter may not be completely independent from the mass accretion rate (e.g. Esin, McClintock & Narayan 1997; Meyer, Liu & Meyer-Hofmeister 2000). Based on the behavior of the 1998 outburst of XTE J1550–564, Homan et al. (2001) claimed that the second independent parameter may be the size of the corona. The transitions may also be a result of an overall change in the type and the geometry of the corona. Zdziarski et al. (2002) explains the different states in Cyg X-1 by the change of an accretion structure which consists of a hot inner accretion flow surrounded by an optically thick disk truncated far away from the minimum stable orbit in the LS, to one that consists of flares and active regions above an accretion disk extending close to the minimum stable orbit in the so-called “soft state”. We note that for Cyg X-1, the soft

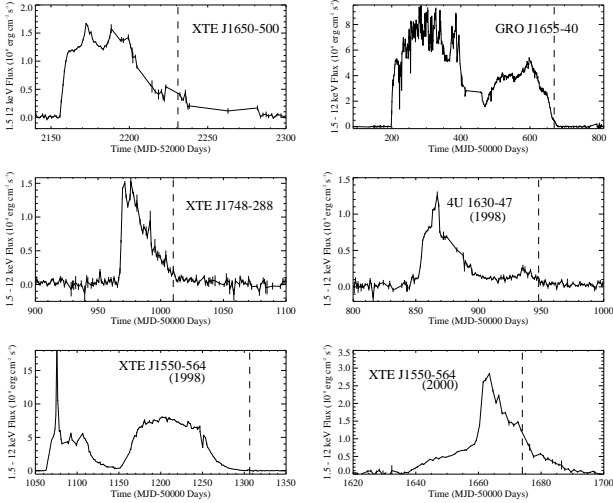


FIG. 1.— The *RXTE*, All Sky Monitor light curves of six outbursts in 1.5–12 keV band. The dashed lines represent the time of transition to the LS during outburst decay.

state is more similar to the IS of GBH transients rather than the HS. According to the hybrid model of Coppi (2000), the state transitions may be explained by a change of size and electron energy distribution of the corona. In the LS, the inner part of the disk puffs up and becomes the hot corona, dominated by thermal electrons. Non-thermal electrons may also be present. In the HS, the edge of the cool accretion disk is close to the minimum stable orbit, and a small, non-thermal corona is also present. In this case, Compton scattering of disk photons by the non-thermal electrons is responsible for the steep power-law observed in the spectra of GBHs in the HS. It has also been claimed that this steep power-law component is a manifestation of Compton up-scattering of disk photons by a converging inflow of material inside the last stable orbit (Laurent & Titarchuk, 2001, and references therein). Then the transition might be related to the type of Comptonization: bulk motion in the HS versus thermal (or hybrid) in the LS.

The transition to the LS not only results in sharp changes in the X-ray spectrum, but also creates a physical environment that shows strong broad-band variability and quasi-periodic oscillations (QPO). The changes in the spectral parameters close to the state transition might provide important clues to understand how this transition is occurring and the driving force of the observed variability. Our group has been observing GBH transients during outburst decays in X-rays with the *Rossini X-ray Timing Explorer (RXTE)* and in radio. We have quantified the evolution before, during and after the transition to the LS for various sources (Kalemci et al., 2001; Tomsick, Corbel & Kaaret, 2001; Kalemci et al., 2003; Tomsick et al., 2003). In Section 3.1, we combine results of spectral and temporal analyses of the *RXTE* data from individual sources during outburst decay using our observations as well as the archival data, and investigate the evolution of the spectral index (Γ), the inner disk temperature (T_{in}), the power-law flux, the disk-blackbody (diskbb) flux and the power-law fraction (PLR, ratio of the power-law flux to the total flux in 3–25 keV band) to obtain a global understanding of the physical environment before and during the state transition.

Another important topic is the evolution of spectral parameters after the state transition, which provides an understanding

of the dynamics of the accretion systems in the LS. In addition to the spectral evolution, the evolution of the temporal parameters is another valuable tool in the LS. Thus, in Section 3.2, we analyze the evolution of spectral and temporal parameters of GBH transients after the state transition. The temporal parameters we use are the characteristic frequencies of the Lorentzian components in the power-spectral-density (PSD) fits and the rms amplitude of variability.

2. OBSERVATIONS AND ANALYSIS

We analyzed the *PCA/RXTE* (Proportional Counter Array, see Bradt, Rothschild & Swank 1993 for a description of *RXTE*) data from all GBH transients that have been observed with *RXTE* between 1996 and 2001 that made a state transition during outburst decay. Eight sources in eleven outburst decays obey these source selection criteria. These sources and outburst years are : XTE J1650–500 in 2001, GRO J1655–40 in 1996, XTE J1748–288 in 1998, XTE J1755–324 in 1997, GX 339–4 in 1998 (decayed in 1999), 4U 1630–47 in 1998, 1999 and 2001, XTE J1550–564 in 1998 and 2000 and XTE J1859+226 in 1999. Although XTE J1755–324 obeys the criteria, it has very poor coverage and results from this source are not included in this work. This decreases the number of sources to seven, and the number of outbursts to ten. Note that XTE J1859+226 did not make a “traditional” transition to the low/hard state, however it showed timing noise for some observations during the decay (see Kalemci 2002 and references therein for the properties and observation times of each source).

For all of the spectral analysis, we fit the data in the 3–25 keV band using the response matrix and the background model created using the standard *FTOOLS* (version 5.2) programs. We added a 1% systematic error to the spectra to account for uncertainties in the *PCA* response. We used a multi-component spectral model consisting of a power-law, a multi-color disk blackbody (**diskbb** in *XSPEC*, Makishima et al., 1986), a broad absorption edge (**smedge** in *XSPEC*, Ebisawa et al., 1994) with interstellar absorption (**phabs** in *XSPEC*). This model has been commonly used for the spectral analysis of GBHs in the LS (Tomsick & Kaaret, 2000; Sobczak et al., 2000). For all observations, the reduced χ^2 is between 0.5 and 1.5. For some observations, in order to reach acceptable χ^2 values, a Gaussian iron line feature was needed. However, the parameters of the iron line have not been used in the analysis. For some of the outbursts, we used published spectral fit parameters if the same model was applied for the fit (Tomsick & Kaaret 2000 for 4U 1630–47 in 1998, and Tomsick, Corbel & Kaaret 2001 for XTE J1550–564 in 2000). All *PCA* fluxes in this report are unabsorbed model fluxes to remove source to source variations due to different absorption column densities. The details of spectral fit models and parameters for each source can be found in Kalemci (2002).

For the temporal analysis, we were as uniform as possible in terms of choosing energy bands, time resolution and segmentation of light curves for all of our sources. However, since some of this work is based on the analysis of the archival data, we were limited to the choice of data modes by the PI of the original proposal. For most of the observations we used 2–26 keV energy band, a Nyquist frequency of 256 Hz and 256 s light curve segments. Although there may be slight differences from source to source in terms of energy band, and highest and lowest PSD frequencies, these differences are not critical since we look for trends rather than absolute values.

Historically, the PSD of GBHs during the low state has

been modeled by a broken power-law (or power-laws with more than one break) plus narrow Lorentzians to fit the QPOs (Nowak et al., 1999; Tomsick & Kaaret, 2000; Kalemci et al., 2001). However, recent papers successfully fit several GBH and neutron star PSDs with broad Lorentzians for the continuum and narrow Lorentzians for the QPOs (Belloni, Psaltis & van der Klis, 2002; van Straaten et al., 2002; Pottschmidt et al., 2003; Kalemci et al., 2003). Following this approach, we fit all our PSDs with Lorentzians of the form:

$$L_i(f) = \frac{R_i^2 \Delta_i}{2\pi [(f - f_i)^2 + (\frac{1}{2} \Delta_i)^2]} \quad (1)$$

where subscript i denotes each Lorentzian component in the fit, R_i is the rms amplitude of the Lorentzian in the frequency band of $-\infty$ to $+\infty$, Δ_i is the full-width-half-maximum, and f_i is the resonance frequency. A useful quantity of the Lorentzian is the “peak frequency” at which the Lorentzian contributes maximum power per logarithmic frequency interval:

$$\nu_i = f_i \left(\frac{\Delta_i^2}{4f_i^2} + 1 \right)^{1/2} \quad (2)$$

Fig. 2 shows an example LS power spectrum of XTE J1650–500 in the form of PSD \times frequency, along with broad and narrow Lorentzians fit components. In this figure, the Lorentzians peak at ν_i , demonstrating the easy identification of characteristic frequencies as peak frequencies of Lorentzian components. Some of our observations contain a Lorentzian that is narrow (with quality value $Q_i = f_i/\Delta_i > 2$, as compared to $Q < 1$ for broad Lorentzians) which we call a QPO. In this work, for each observation, the term “characteristic frequency” represents the resonance frequency of the fundamental QPO⁶ if present, and otherwise the lowest peak frequency of the broad Lorentzian components in the PSD⁷. Note that since the QPO frequencies

⁶The peak frequency and the resonance frequency differ by $<3\%$ for QPOs with $Q > 2$.

⁷The lowest peak frequency is nearly equivalent to the “break frequency” if broken power-law modeling is adopted, see Belloni, Psaltis & van der Klis (2002) for a detailed discussion.

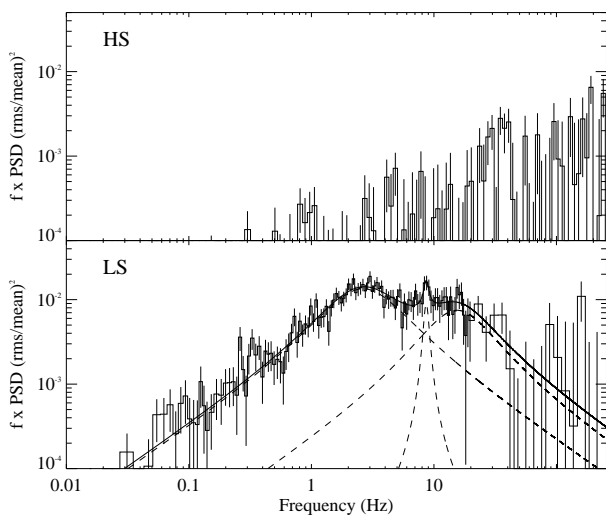


FIG. 2.— Power spectra of XTE J1650–500 in the HS (top panel) and in the LS (bottom panel). The PSD in the LS is fitted with two broad and a narrow Lorentzian. The HS observation has a 2σ upper limit of 4% on the rms amplitude of variability, whereas the LS observation 2 days later has an rms amplitude of variability of $12.43 \pm 0.55\%$

and the Lorentzian peak frequencies are all shown to be correlated (Belloni, Psaltis & van der Klis, 2002), it does not matter which one we use to characterize the evolution. The rms amplitudes are calculated over a frequency band from zero to infinity.

Mostly due to our group’s monitoring program of GBHs, with *RXTE* during outburst decay, we obtained very good coverage for 3 sources, in 6 different outbursts (1998, 1999 and 2001 outbursts of 4U 1630–47, 1998 and 2000 outbursts of XTE J1550–564, and the 2001 outburst of XTE J1650–500 with almost daily monitoring). GRO J1655–40 and GX 339–4 are excluded from the discussion of the changes before and during the transition in Section 3.1 since they have poor coverage (≥ 10 days between observations). XTE J1748–288 with observations every ~ 5 days is included in the discussion of the evolution to the state transition, however is not included in the discussion of the changes during the transition. Results from these sources are included in the discussion of the evolution after the transition for which very good coverage is not necessary. All the data used in this report are available on-line as a machine-readable table.

3. RESULTS

In this work, we define the state transition in terms of sharp changes in variability properties rather than sharp changes in spectral properties. All of our sources with good coverage showed sharp, distinct changes in terms of variability in less than two days, but this was not the case for the spectral properties. Most of the transitions occurred from the HS to LS, and for those cases the transition was marked by a very large increase in the total rms amplitude of variability as shown in Fig. 3a. For most of the cases, the transition was from a featureless, Poisson noise dominated PSD with only a few % rms amplitude upper limit to a PSD showing well defined broadband variability. In other words, the variability “appeared” on a few days timescale for these systems. Fig. 2 represents this appearance of variability, as the observation in the HS (top panel, with $<4\%$ rms upper limit variability) and the observation in the LS (bottom panel, with $>12\%$ rms variability with well defined Lorentzian components and a QPO) in this figure are only two days apart. Since the HS PSD is often featureless and has very low or no rms amplitude of variability, it is not possible to discuss the evolution of characteristic frequencies before the transition for none of our sources except the 2000 outburst of XTE J1550–564, which showed a complex pattern. It was in the IS, with rms amplitude variability of $\sim 13\%$. During the IS, it showed a QPO with constant frequency at ~ 9 Hz. Then it showed a large drop in variability to an amplitude of $\sim 7\%$. We marked this change as the transition. Two days later, the rms amplitude of variability jumped again to levels of 15%. The morphology of the PSDs was different in the IS, LS, and during the time that the rms amplitude showed a drop (Kalemci, 2002). Despite the complexity of some individual cases, it is possible to infer global patterns of evolution for different parameters before, during and after the state transition.

3.1. Changes in spectral properties that lead to state transitions

First, we characterize the changes in spectral properties before the state transition. The evolution of the photon spectral index (Γ), and the inner disk temperature (T_{in}) close to the transition are shown in Fig. 3b and c respectively. The evolution of the PLR, power-law flux and the diskbb flux are shown in Fig. 4. In most sources, Γ (Fig. 3b) is approximately constant

until 3-5 days before the timing transition at which point it begins to decline. For some sources, there is a distinct drop in Γ at the beginning of the decline. Except for the 1998 outburst of XTE J1550–564, T_{in} (Fig. 3c) either decreases or stays constant before the transition. The power-law flux (Fig. 4b) shows a complex behavior (see also Fig. 5), and the diskbb-flux (Fig. 4c) decreases for majority of the outbursts, or stays constant. The cumulative effect of the power-law and diskbb-flux evolution for the majority of the outbursts is an increasing PLR (Fig. 4a) before the transition.

We established that the transition occurs in a few days time scale for GBH transients. The change in variability properties (usually, the appearance of variability) that defines the transition should be a response to the change of one or more spectral parameters. To understand which parameter drives the transitions and appearance of variability, we compared the two observations just before and after the transition (observations just before and after the dashed lines in Figs. 3 and 4). We specify that a spectral parameter is showing a sharp change during the transition if either the slope of the parameter as a function of time changes sign or the percentage change in the value of the parameter compared to the previous observation is at least three times that of the previous observation. With this definition, two parameters show a sharp change for the majority of the outbursts: the power-law flux (see Fig. 5) and the PLR⁸. The PLR is not an independent parameter, and in this case its increase is mostly driven by the increase in the power-law flux. For both the 1999 and the 2001 outbursts of 4U 1630–47, there is no

⁸GX 339–4 during its recent decay from the outburst showed a large increase in the PLR, and by using this information, we were able to estimate when the transition would occur and scheduled a successful *RXTE* observation to catch the beginning of the transition.

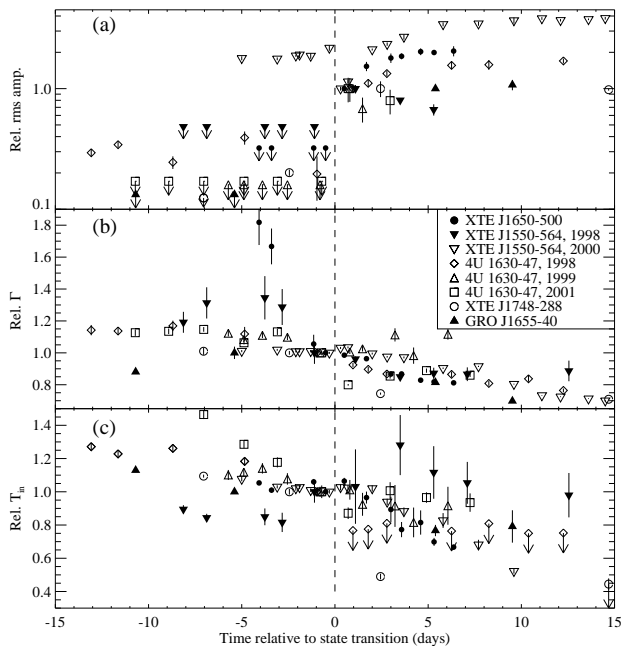


FIG. 3.— Evolution of (a) the rms amplitude of variability, (b) the spectral index, and (c) the inner disk temperature. The state transition is assumed to have happened exactly in between the observations closest to the sharp change observed in panel (a), and represented by a dashed line. For (a), the values for each source are normalized with respect to the value just after the state transition. For both (b) and (c), the values for each source are normalized with respect to the value just before the state transition. For some points, the 1σ errors are smaller than the plot symbols. The upper limits are 2σ .

sharp change in any of the spectral parameters between those two observations, yet one observation shows no variability and the next one shows variability. However, for both, the evolution of the power-law flux shows a change in the slope an observation earlier. The situation is more complicated for the 2000 outburst of XTE J1550–564. There is a large increase in the power-law flux and PLR during the transition, but this change corresponds to a decrease in the rms amplitude (Kalemci, 2002).

Analysis of PCA data from GBH transient XTE J1859+226 during its outburst decay revealed interesting behavior in terms of variability and spectral evolution and provided another case for the relation between the power-law flux and variability. XTE J1859+226 did not show a traditional transition, but showed variability for some of the observations during the decay. In 1 day timescale, the power-law flux almost doubled and variability appeared, and when the power-law flux dropped below a threshold value, variability disappeared. Except the PLR, which is tied to the power-law flux, no other spectral parameter showed a sharp change between observations that show variability, and those that do not show variability for this source (Kalemci, 2002).

3.1.1. A discussion of transition fluxes

It is important to get an idea of when the transition happens during the decay for effective monitoring of the sources with pointed instruments. Often the sources are not monitored frequently enough (i.e., once a day) with pointed observations, but the ASM measures the flux in 3 energy bands very frequently, which provides an opportunity to detect transitions without re-pointing the satellite. (See Fig. 1 for the ASM light curves of some of our sources.) The transition is often detected by a sudden increase in the hardness ratio 2 (HR2, the ratio of 5–12 keV flux to 1.5–3 keV flux). A few days just before and after the transition may manifest the most interesting behavior. A

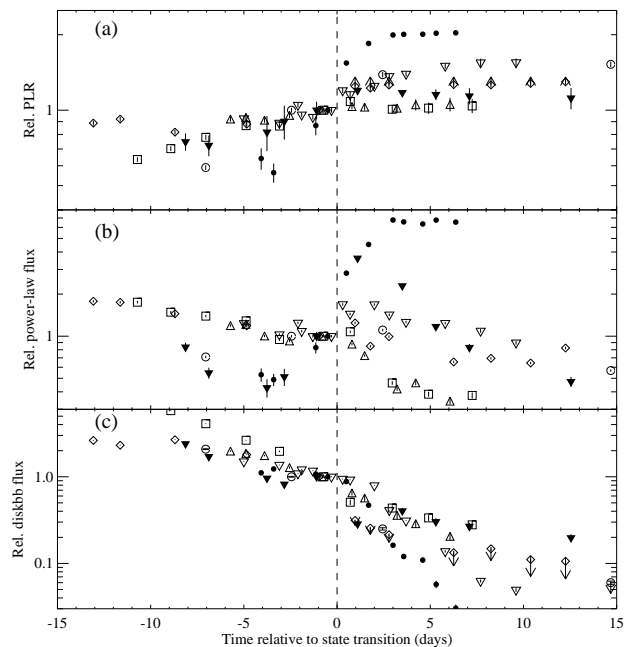


FIG. 4.— Evolution of (a) the PLR, (b) the power-law flux, and (c) the diskbb flux. The dashed line represents the time of transition. The values for each source are normalized with respect to the value just before the state transition. A legend is given in Fig. 3. For some points, the 1σ errors are smaller than the plot symbols. The upper limits are 2σ .

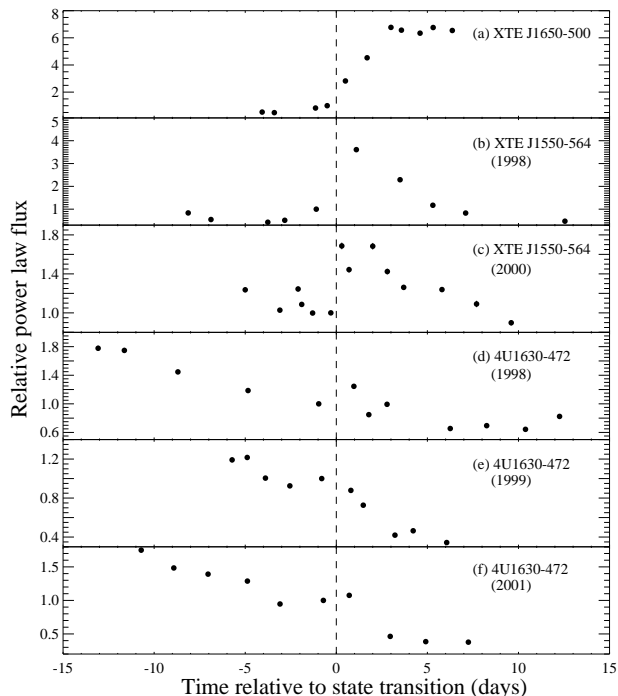


FIG. 5.— Evolution of the power-law flux before and after the transition. The dashed line indicates the time of state transition. The values for each source are normalized with respect to the value just before the state transition. The 1σ errors are smaller than the plot symbols

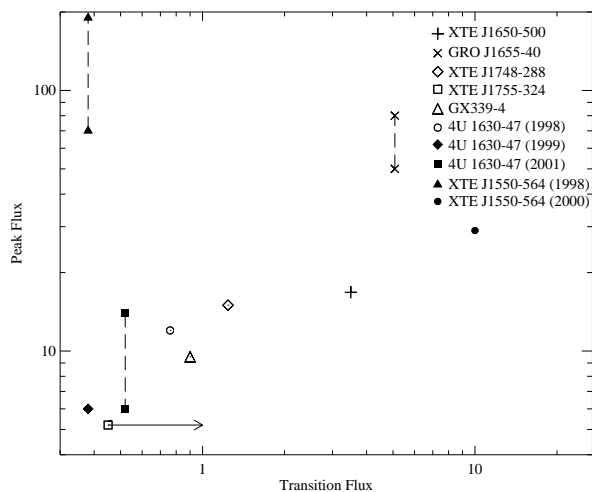


FIG. 6.— Peak flux versus transition flux in 1.5 – 12 keV band. Fluxes are in units of 10^{-9} ergs cm^{-2} s^{-1} . For the points connected with dashed lines, both peak fluxes and plateau fluxes are shown.

relationship between the peak flux and the transition flux (1.5 – 12 keV flux for the observation that shows variability) had been realized earlier (Tomsick, private communication). We plot this relation for all of the outbursts that show a state transition in Fig. 6. Except the 1998 outburst of XTE J1550–564, which showed one of the strongest flares in the *RXTE* history, the transition flux increases with the peak flux. The Spearman’s rank order correlation coefficient for this data set (excluding the 1998 outburst of XTE J1550–564) is 0.90, pointing out a correlation. On the other hand, the linear correlation coefficient is 0.52, indicating a relation which is not strictly linear.

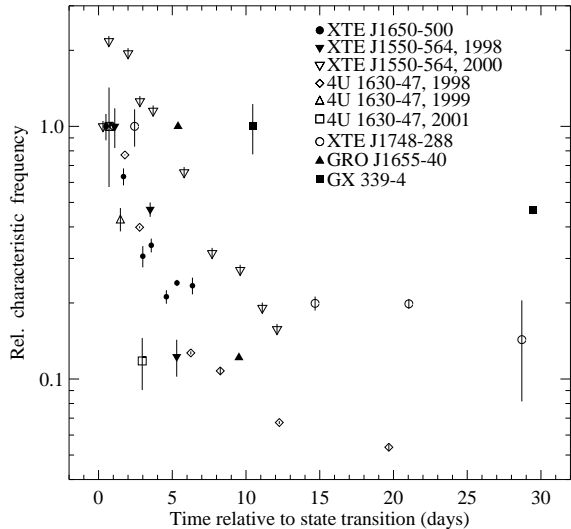


FIG. 7.— Evolution of the characteristic frequencies (the QPO resonance frequency for XTE J1550–564 in 2000, 4U 1630–47 in 1998 and 1999, and XTE J1748–288, lowest peak frequency of the broad Lorentzian components in the PSD for the remaining) after the state transition. For some points, the 1σ errors are smaller than the plot symbols.

Some outbursts have the usual “fast-rise-exponential-decay” (FRED) shape (such as XTE J1748–288), and some have a very complicated shape (such as 4U 1630–47 in 2001). The complicated ones may show a plateau before the final decay (like GRO J1655–40, and XTE J1550–564 in 2000 in Fig. 1). For these sources, we also plotted the plateau ASM flux along with the peak flux. Replacing the peak flux by the plateau flux for these sources improves the linear correlation for the whole sample to r of 0.706. The linear correlation is not very strong, but it allows for an estimate of when the transition might happen, which is useful for planning observations to study the transition.

3.2. Evolution of spectral and temporal parameters after the transition

The evolution of spectral and temporal parameters after the transition is shown in Figs. 3, 4, 5, and 7. For XTE J1650–500, GX 339–4 (not shown in Figs. 3, 4, 5 because of poor coverage), 4U 1630–47 in 1998 and XTE J1550–564 in 2000, Γ decreases after the transition. For other outbursts, it is either constant or shows irregular behavior. The power-law flux decreases for all of the outbursts except XTE J1650–500 (see Figs. 4 and 5). For most cases, the diskbb-flux and T_{in} either decrease, or are unobservable after the transition. It is hard to constrain the evolution of T_{in} for the 1998 outburst of XTE J1550–564 and the 2001 outburst of 4U 1630–47. For all outbursts, the diskbb component is unobservable within 15 days of the state transition. For XTE J1650–500 and the 2000 outburst of XTE J1550–564, the PLR first increases and then stays constant. For all other outbursts, the PLR is very close to unity and does not vary.

The evolution of the characteristic frequencies after the transition is shown in Fig. 7. Except a single observation at the beginning of the 2000 outburst of XTE J1550–564, all characteristic frequencies decrease after the transition. There are only two observations that show variability in the 1999 and 2001 outbursts of 4U 1630–47, and even for those cases, the later observations have smaller characteristic frequencies. The behavior

of the rms amplitudes are more complicated (see Fig. 3a). The 1998 outburst of XTE J1550–564 and XTE J1748–288 show a decreasing trend. The rms amplitudes for XTE J1650–500, the 2000 outburst of XTE J1550–564 and the 1998 outburst of 4U 1630–47 increase and level off. For GRO J1655–40, the rms amplitudes are consistent with being constant. For GX 339–4 on the other hand, the rms amplitude increases Kalemci (2002).

4. DISCUSSION

4.1. State transition and appearance of variability

First, we discuss possible reasons for the state transition and appearance of variability based on our results above. Suppose almost all of the variability we observe is due to the photons coming from the power-law component presumably originating in the corona, and the disk photons are providing mostly Poisson noise. This idea is supported by the fact that very little or no variability is observed during the HS when the diskbb dominates, and strong variability is observed when the power-law component dominates in the LS. The anti-correlation between the diskbb flux and the rms amplitude observed both in XTE J1650–500 (Kalemci et al., 2003) and the 2000 outburst of XTE J1550–564 (Kalemci et al., 2001) is also potentially consistent with this scenario. It is conceivable that the Poisson noise dominated diskbb flux reduces the rms amplitudes of variability to unobservable levels. Then the PLR would be a good indicator of when the variability will be observed, since the higher the PLR, the lower the diskbb flux compared to the total flux. For all of our sources, no variability is observed if the $PLR < 0.45$. However, the value of the PLR cannot be the sole determinant of when the variability will be observed. For most of the sources the PLR has to be greater than 0.8 for the variability to appear, although it can be as low as 0.45 for XTE J1859+226 (Kalemci, 2002). To test the argument that the diskbb flux might reduce the rms amplitudes to unobservable levels, we conducted very simple simulations. We added various levels of Poisson noise to the light curve of an observation of GRO J1655–40 taken on August 14, 1997, and compared the resultant PSD with the original PSD. We chose this observation since it has a complex structure, and no diskbb flux, so all the emission is coming from the corona. The results are shown in Fig. 8. Although this figure clearly shows that the rms amplitude of the PSD depends on the PLR, it also shows that even for a PLR of 0.3, the variability is clearly observed. There is no large change in the PSD shape. Moreover, lack of diskbb emission **does not** guarantee broad-band variability even if a hard component exists. There is strong emission in the 6–15 keV band for most of the sources before the transition, and spectral analysis shows that only a few percent of the emission in this band is from the soft component. Nonetheless, although completely power-law dominated, these observations do not show variability. Note that, these simple simulations do not take into account the effects of strong disk emission on the corona. The two emission components are not independent of each other, because Compton cooling of the corona by the diskbb emission can affect the temperature and density structure of the corona. The amount of diskbb radiation cannot be ruled out as an important parameter in determining when the variability will be observed.

The power-law emission dominates the LS when the variability is observed but its presence alone is not enough to create broad-band variability. These findings suggest several possibilities for the presence of variability in the LS. The origin of the

power-law component in the LS and the other states might be completely different. The passage from the IS to the LS (as observed for GX 339–4 and the 2000 outburst of XTE J1550–564) might be due to a change of the form of the corona from active regions above the accretion disk to an inner accretion flow (Zdziarski et al., 2002). The power-law component in the HS may be a result of Comptonization of disk photons by non-thermal electrons (Coppi, 2000), or bulk motion Comptonization (Laurent & Titarchuk, 2001), whereas in the LS, it may be due to thermal Comptonization. However, if the form or the composition of the corona is changing during the transition, one would expect a sharp change not only in power-law flux, but also in Γ , especially if the change is from bulk motion Comptonization to thermal Comptonization. There are two ways to increase the power-law flux: increasing the number of seed photons; and/or increasing the area of the corona that intercepts the seed photons. It is unlikely that the number of seed photons are increasing, the corona is believed to be optically thin, and an increase in the soft flux should be observed (unless most photons have energies below the PCA range). Therefore, our findings are consistent with the idea that, during the transitions, the size of the corona increases to a threshold value for variability, which would be consistent with the idea that the second independent parameter determining the spectral states is the size of the Comptonizing region (Homan et al., 2001). The strongest support for this explanation comes from the behavior of XTE J1859+226. Variability appeared for this source whenever the power-law flux is higher than a threshold value. No other spectral variable shows a significant change between observations with and without variability (Kalemci, 2002). The only caveat of this scenario is the resemblance of the variability properties of XTE J1859+226 to the IS observations of GX 339–4 and the 2000 outburst of XTE J1550–564, rather than to the LS properties.

An increase in the power-law flux does not always correspond to the appearance of variability. The 2000 outburst of

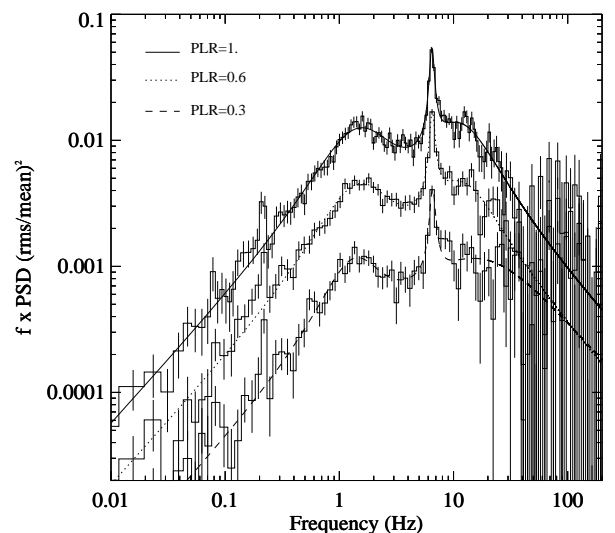


FIG. 8.— PSD of GRO J1655–40 during an observation in the LS is shown with the solid curve obtained by fitting the PSD with two broad Lorentzians and a QPO. The dotted and the dashed curves are fits to the PSDs when Poisson noise is added to the original light curve. The PSD under the dotted curve corresponds to a PLR of 0.6 and the PSD under the dashed curve corresponds to a PLR of 0.3.

XTE J1550–564 behaved differently; the rms amplitude of variability decreased as the the power-law flux increased sharply. But in a couple of days after the first transition, another transition happened and strong variability that is usually associated with the LS appeared. The 1999 and the 2001 outbursts of 4U 1630–47 did not show a sharp change in any of the spectral properties at the transition (see Figs. 3 and 4), but both showed a change in the slope of the evolution of the power-law flux an observation earlier (see Fig. 5). This suggests the possibility that for some cases the appearance of variability (in the case of XTE J1550–564, variability associated with the LS) is delayed. The transition for these cases may be happening slower than that of other cases, and during the restructuring of the accretion geometry, the coherence could be lost for all timescales and the timing signatures could be suppressed for a few days.

4.2. Evolution of spectral and temporal parameters

Two important observations about the transitions to the LS can be made by analyzing the evolution of spectral parameters before the transition. First, the PLR increases for the majority of the outbursts. The corona (again assumed to be the source of the power-law flux) must dominate for the transition to happen, the PLR is greater than 0.65 for all sources after the transition to the LS. The PLR was as low as 0.45 for XTE J1859+226 when the variability was observed, but it never made the transition to the canonical LS, and returned back to the HS when the PLR dropped (Kalemci, 2002). Second, the spectral indices for some of the sources show a step function-like decrease 3-5 days before the transition (see Fig. 3b). This may be interpreted as the time of spectral transition, which would indicate that the transition in timing properties lags the transition in spectral properties. Then, the change in Γ may be a sign of changing the form of the corona as discussed in the previous section, and the lag between the change in the Γ and the appearance of variability is the time for the corona to reach a threshold volume. However, some sources do not show any drop in Γ , but still show a sharp change in temporal variability (Fig. 3a), making the transitions much easier to identify.

After the transition, the evolution of the inner disk temperature, the diskbb flux, the power-law index and especially the characteristic frequencies of the variability are consistent with the idea of the inner disk retreat. In the basic formulation of Makishima et al. (1986), the optically thick disk has a temperature profile that decreases with increasing radius. Therefore, if the inner disk evaporates as part of the transition, it is expected that both T_{in} and diskbb flux decrease. Most sources show a decrease in diskbb flux, and at least four sources show a decrease in T_{in} . The drop of spectral index may also be a sign of increasing inner disk radius. As the disk is closer to the black hole, its temperature and flux are higher, causing effective cooling of the corona, increasing the spectral index (Zdziarski et al., 2002). Four sources show a decreasing Γ . It is intuitively expected that the characteristic frequencies decrease as the inner disk radius increases. The dynamical timescale (the fastest timescale) in the accretion disk is shorter close to the black hole, and it is expected that higher frequency variability is created in this region. As the inner disk radius retreats (or the inner disk evaporates) the dynamical timescale (at the inner edge) increases, and therefore the characteristic frequencies in the PSD decrease. The exact relation between the characteristic frequencies and the dynamical timescales is not clear yet. All sources show a decreasing behavior in terms of characteristic frequencies, except for one observation. The overall evolution of both spectral

and temporal properties therefore indicates that the inner edge of the accretion disk retreats as the system progresses in the LS, in accordance with the model of Esin, McClintock & Narayan (1997). In the exceptional case, the QPO frequencies in the 2000 outburst of XTE J1550–564 first increased and then decreased after the transition (see Fig. 7). This behavior is consistent with the prediction of the “accretion ejection instability” QPO model (Tagger & Pellat, 1999) if the inner accretion disk is close to the marginally stable orbit during this observation. This possibility is discussed in detail in Rodriguez et al. (2002) and Kalemci (2002).

The interpretation of the behavior of the rms amplitudes is more complex. We showed the relation between the PLR and the rms amplitudes earlier (see Fig. 8). The “Poissonic” nature of the disk component causes a decrease in the rms amplitudes at lower energies due to the diskbb energy spectrum peaking at those energies. This might explain the increase and leveling of the rms amplitudes in XTE J1650–500 and the 2000 outburst of XTE J1550–564. Although the rms amplitudes seem to be decreasing after the transition for the 1998 outburst of XTE J1550–564, it might be a result of not constraining the high frequency part of the PSD. The first observation requires two Lorentzians to fit, and results in a high PSD amplitude, whereas for the remaining observations, the second Lorentzian, although statistically not required, cannot be excluded (Kalemci, 2002). The fits are better for XTE J1748–288 and it also shows a decreasing behavior. The interpretation of the rms amplitudes of XTE J1748–288 is complicated due to the high absorption column density. The Galactic ridge emission may also be affecting the rms amplitudes at low flux levels by supplying additional Poissonic emission. The rms amplitude of GX 339–4 increases after the transition although there is no diskbb flux in the 3-25 keV band. Overall, there is no definite trend of evolution for the rms amplitudes after the transition.

5. SUMMARY

An important goal of black hole binary research is to understand the accretion structure and nature of variability of these systems. This work addresses these goals by analyzing the X-ray temporal and spectral properties of a relatively large subset of GBHs during outburst decay. We characterize the evolution of spectral and temporal properties before and after the transitions, and also work on the changes right at the transition to understand the appearance of broad-band variability.

For this study, a total of seven *RXTE* sources in ten outbursts are analyzed. Thanks to our group’s monitoring program, the coverage close to the transition is significantly improved, and for the first time allows us to determine the physical changes that drive the transitions in detail. The first problem we work on is the evolution of spectral parameters before the state transition and appearance of broad-band variability at the state transition. We show that the changes in variability properties (a sudden increase or decrease in the rms amplitude of variability) are sharper than changes in spectral properties, and it is easier to identify a transition with the temporal properties. A change in the spectral index Γ is shown to be the pre-cursor of the transition showing a decrease 3-5 days before for most of our sources. We also show that the PLR increases close to the transition for all sources. The hard power-law component must dominate the spectrum for the transition to happen. Very frequent monitoring observations (\sim once a day) allow us to determine the power-law flux (and consequently the PLR) as the parameter showing a sharp change during the transitions which

may indicate a threshold volume for the corona for the appearance of variability.

We also investigate the evolution after the state transition. For most of the cases, the T_{in} and the diskbb flux decrease after the transition, and they are unobservable with PCA within fifteen days of the transition for all outbursts. The characteristic frequencies of all except one observation of the 2000 outburst of XTE J1550–564 decrease after the state transition. These spectral and temporal changes are consistent with the idea that the inner accretion disk retreats after the state transition. The rms amplitude of variability does not show any global trend with time after the transition, and its behavior is consistent with the emission from the soft component having no or very little temporal signature.

E.K. acknowledges useful discussions with David Smith, Ali Alpar and Ünal Ertan. The majority of this work was done at the Center for Astrophysics and Space Sciences (CASS) at UCSD as part of E.K.'s dissertation. E.K. acknowledges the support of the Astrophysics Forum at Sabancı University where a portion of this work was prepared, and also acknowledges partial support of TÜBİTAK. The authors would like to thank all scientists contributed to the Tübingen Timing Tools. J.A.T. acknowledges partial support from NASA grant NAG5-13055. K.P. was supported by grant Sta 173/25-1 and Sta 173/25-3 of the Deutsche Forschungsgemeinschaft. P.K. acknowledges partial support from NASA grant NAG5-7405. This work was also supported by NASA contract NAS5-30720.

References

- Belloni, T., Psaltis, D., & van der Klis, M., 2002, *ApJ*, 572, 392
- Bradt, H. V., Rothschild, R. E., & Swank, J. H., 1993, *A&AS*, 97, 355
- Coppi, P. S., 2000, in *High Energy Processes in Accreting Black Holes*, ASP Conf. Ser. 161: High Energy Processes in Accreting Black Hole, eds. Poutanen, J. and Svensson, R., (1999)
- Corbel, S., et al., 2001, *ApJ*, 554, 43
- Ebisawa, K., et al., 1994, *PASJ*, 46, 375
- Esin, A. A., McClintock, J. E., & Narayan, R., 1997, *ApJ*, 489, 865
- Fender, R. P., Hjellming, R. M., Tilanus, R. P. J., Pooley, G. G., Deane, J. R., Ogle, R. N., & Spencer, R. E., 2001, *MNRAS*, 322, L23
- Homan, J., Wijnands, R., van der Klis, M., Belloni, T., van Paradijs, J., Klein-Wolt, M., Fender, R., & Méndez, M., 2001, *ApJS*, 132, 377
- Kalemci, E., 2002, *Ph.D. Thesis*, University of California, San Diego
- Kalemci, E., Tomsick, J. A., Rothschild, R. E., Pottschmidt, K., Corbel, S., Wijnands, R., Miller, J. M., & Kaaret, P., 2003, *ApJ*, 586, 419
- Kalemci, E., Tomsick, J. A., Rothschild, R. E., Pottschmidt, K., & Kaaret, P., 2001, *ApJ*, 563, 239
- Laurent, P., & Titarchuk, L., 2001, *ApJ*, 562, L67
- Makishima, K., Maejima, Y., Mitsuda, K., Bradt, H. V., Remillard, R. A., Tuohy, I. R., Hoshi, R., & Nakagawa, M., 1986, *ApJ*, 308, 635
- McClintock, J. E., & Remillard, R. A., 2003, in *X-ray Binaries*, astro-ph/0306213
- Meyer, F., Liu, B. F., & Meyer-Hofmeister, E., 2000, *A&A*, 361, 175
- Miyamoto, S., Kitamoto, S., Hayashida, K., & Egoshi, W., 1995, *ApJ*, 442, LL13
- Nowak, M. A., 2002, in *Proceedings of the 4th Microquasar Workshop, 2002*, eds. Durouchoux, Fuchs, Rodriguez, to be published by the Center for Space Physics: Kolkata, 7624
- Nowak, M. A., Vaughan, B. A., Wilms, J. ., Dove, J. B., & Begelman, M. C., 1999, *ApJ*, 510, 874
- Pottschmidt, K., et al., 2003, *A&A*, 407, 1039
- Rodriguez, J., Corbel, S., Kalemci, E., Tomsick, J. A., & Tagger, M., 2002, submitted to *ApJ*
- Sobczak, G. J., McClintock, J. E., Remillard, R. A., Cui, W., Levine, A. M., Morgan, E. H., Orosz, J. A., & Bailyn, C. D., 2000, *ApJ*, 544, 993
- Tagger, M., & Pellat, R., 1999, *A&A*, 349, 1003
- Tanaka, Y., & Lewin, W. H. G., 1995, in *X-ray Binaries*, ed. W. H. G. Lewin, J. Van Paradijs, E. P. J. Van den Heuvel, (Cambridge: Cambridge U. Press), 126
- Tomsick, J. A., Corbel, S., & Kaaret, P., 2001, *ApJ*, 563, 229
- Tomsick, J. A., & Kaaret, P., 2000, *ApJ*, 537, 448
- Tomsick, J. A., Kalemci, E., Corbel, S., & Kaaret, P., 2003, *ApJ*, 592, 1100
- van Straaten, S., van der Klis, M., di Salvo, T., & Belloni, T., 2002, *ApJ*, 568, 912
- Zdziarski, A. A., Poutanen, J., Paciesas, W. S., & Wen, L., 2002, *ApJ*, 578, 357

TABLE 1
PARAMTERS FOR XTE J1650–500^a

^aThis table is available only on-line as a machine-readable table.

Obs.	Date ^a	Γ	T_{in}	Power law Fl.	Dbb Fl.	PLR	rms (%)	ν_1 ^b	QPO Freq. ^c
1	52227.5	4.390 ± 0.343	0.484 ± 0.002	2.400 ± 0.264	5.255 ± 0.052	0.313 ± 0.030	<4 ^d	-	-
2	52228.1	4.026 ± 0.271	0.464 ± 0.007	2.211 ± 0.221	5.822 ± 0.058	0.275 ± 0.024	<4	-	-
3	52230.4	2.548 ± 0.140	0.487 ± 0.008	3.747 ± 0.337	5.080 ± 0.050	0.424 ± 0.036	<4	-	-
4 ^e	52231.0	2.415 ± 0.038	0.459 ± 0.004	4.524 ± 0.135	4.731 ± 0.047	0.488 ± 0.015	<4	-	-
5	52232.0	2.379 ± 0.019	0.489 ± 0.009	12.76 ± 0.127	4.171 ± 0.041	0.753 ± 0.009	12.42 ± 0.546	4.162 ± 0.498	-
6	52233.2	2.326 ± 0.023	0.443 ± 0.016	20.49 ± 0.204	2.221 ± 0.022	0.902 ± 0.010	19.01 ± 1.672	2.634 ± 0.202	8.734 ± 0.219
7	52234.5	2.093 ± 0.011	0.410 ± 0.035	30.62 ± 0.306	0.767 ± 0.030	0.975 ± 0.012	22.28 ± 1.992	1.274 ± 0.123	5.131 ± 0.090
8	52235.1	2.096 ± 0.009	0.355 ± 0.021	29.70 ± 0.297	0.569 ± 0.022	0.981 ± 0.012	23.04 ± 1.287	1.408 ± 0.089	5.440 ± 0.087
9	52236.1	2.001 ± 0.009	0.374 ± 0.033	28.70 ± 0.287	0.517 ± 0.036	0.982 ± 0.012	25.16 ± 1.614	0.881 ± 0.054	4.655 ± 0.072
10	52236.9	1.976 ± 0.007	0.321 ± 0.011	30.58 ± 0.305	0.271 ± 0.027	0.991 ± 0.012	24.75 ± 0.330	0.999 ± 0.028	3.799 ± 0.034
11	52237.9	1.961 ± 0.008	0.306 ± 0.006	29.59 ± 0.295	0.144 ± 0.014	0.995 ± 0.012	25.45 ± 2.449	0.974 ± 0.073	3.830 ± 0.077

^aMJD, Modified Julian Date, same for all Tables

^bLowest peak frequency, same for all Tables.

^cResonance frequency of the QPO if present, same for all Tables.

^dAll upper limits are 2 σ in all Tables.

^eThe state transition happened between this observation and the next observation. The values in Figs. 3, 4, 5 are normalized using parameters in this observation. Fig. 7 observations are normalized with respect to the next observation. Same for all tables.

TABLE 2
PARAMTERS FOR XTE J1550–564 IN 1998

Obs.	Date	Γ	T_{in}	Power law Fl.	Dbb Fl.	PLR	rms (%)	ν_1	QPO Freq.
1	1298.09	2.439 ± 0.134	0.415 ± 0.011	0.867 ± 0.065	0.547 ± 0.010	0.613 ± 0.048	<10	-	-
2	1299.34	2.688 ± 0.200	0.392 ± 0.011	0.567 ± 0.051	0.389 ± 0.007	0.593 ± 0.055	<10	-	-
3	1302.46	2.754 ± 0.278	0.394 ± 0.023	0.444 ± 0.066	0.219 ± 0.004	0.669 ± 0.106	<10	-	-
4	1303.39	2.635 ± 0.230	0.379 ± 0.027	0.532 ± 0.074	0.187 ± 0.005	0.739 ± 0.114	<10	-	-
5	1305.12	2.047 ± 0.141	0.464 ± 0.030	1.038 ± 0.072	0.228 ± 0.006	0.819 ± 0.066	<10	-	-
6	1307.32	1.968 ± 0.031	0.479 ± 0.104	3.746 ± 0.074	0.065 ± 0.005	0.982 ± 0.024	22.13 ± 1.590	1.175 ± 0.210	-
7	1309.72	1.739 ± 0.036	0.595 ± 0.084	2.377 ± 0.047	0.092 ± 0.007	0.962 ± 0.024	17.74 ± 0.600	0.551 ± 0.036	-
8	1311.52	1.785 ± 0.071	0.518 ± 0.073	1.216 ± 0.048	0.069 ± 0.006	0.946 ± 0.047	14.81 ± 1.590	0.144 ± 0.024	-
9	1313.32	1.773 ± 0.088	0.489 ± 0.058	0.861 ± 0.051	0.061 ± 0.006	0.933 ± 0.068	<8	-	-
10	1318.77	1.815 ± 0.132	0.455 ± 0.062	0.491 ± 0.039	0.045 ± 0.004	0.916 ± 0.089	<8	-	-

TABLE 3
PARAMTERS FOR XTE J1550–564 IN 2000

Obs.	Date	Γ	T_{in}	Power law Fl.	Dbb Fl.	PLR	rms (%)	ν_1	QPO Freq.
1	51667.7	2.368 ± 0.016	0.798 ± 0.010	6.221 ± 0.124	4.539 ± 0.045	0.578 ± 0.012	12.50 ± 0.470	10.01 ± 1.264	9.030 ± 0.240
2	51669.6	2.386 ± 0.014	0.763 ± 0.007	5.170 ± 0.103	4.142 ± 0.041	0.555 ± 0.012	12.37 ± 0.330	9.571 ± 0.894	8.160 ± 0.136
3	51670.6	2.363 ± 0.014	0.756 ± 0.010	6.263 ± 0.125	3.307 ± 0.033	0.654 ± 0.014	13.12 ± 0.280	9.951 ± 0.601	9.320 ± 0.088
4	51670.8	2.362 ± 0.015	0.761 ± 0.008	5.467 ± 0.109	3.669 ± 0.036	0.598 ± 0.013	13.36 ± 0.840	9.615 ± 0.932	8.610 ± 0.116
5	51671.4	2.366 ± 0.017	0.748 ± 0.008	5.022 ± 0.100	3.550 ± 0.035	0.585 ± 0.012	13.06 ± 0.690	9.699 ± 0.653	-
6	51672.4	2.342 ± 0.015	0.741 ± 0.008	5.031 ± 0.100	3.030 ± 0.030	0.624 ± 0.013	15.21 ± 0.790	8.906 ± 0.768	8.810 ± 0.141
7	51673.0	2.414 ± 0.015	0.761 ± 0.014	8.486 ± 0.169	2.857 ± 0.028	0.748 ± 0.017	7.230 ± 0.260	5.959 ± 1.037	-
8	51673.4	2.422 ± 0.014	0.759 ± 0.012	7.261 ± 0.145	2.798 ± 0.027	0.721 ± 0.016	8.440 ± 0.290	6.735 ± 1.076	-
9	51674.7	2.331 ± 0.014	0.756 ± 0.014	8.471 ± 0.169	2.400 ± 0.024	0.779 ± 0.017	14.77 ± 0.290	1.019 ± 0.257	3.580 ± 0.015
10	51675.5	2.284 ± 0.012	0.696 ± 0.014	7.164 ± 0.143	1.245 ± 0.012	0.851 ± 0.019	16.38 ± 0.520	1.794 ± 0.137	7.690 ± 0.089
11	51676.4	2.275 ± 0.014	0.654 ± 0.017	6.346 ± 0.126	0.942 ± 0.009	0.870 ± 0.020	18.77 ± 0.960	2.425 ± 0.429	6.930 ± 0.020
12	51678.5	2.116 ± 0.011	0.613 ± 0.033	6.233 ± 0.124	0.417 ± 0.012	0.937 ± 0.022	23.88 ± 0.890	1.148 ± 0.092	4.490 ± 0.014
13	51680.4	2.143 ± 0.009	0.505 ± 0.022	5.489 ± 0.164	0.190 ± 0.007	0.966 ± 0.035	24.19 ± 0.950	1.014 ± 0.083	4.090 ± 0.015
14	51682.3	1.883 ± 0.007	0.387 ± 0.011	4.520 ± 0.135	0.150 ± 0.007	0.967 ± 0.035	25.70 ± 1.530	0.558 ± 0.029	2.340 ± 0.010

TABLE 4
PARAMTERS FOR 4U 1630–47 IN 1998

Obs.	Date	Γ	T_{in}	Power law Fl.	Dbb Fl.	PLR	rms (%)	ν_1	QPO Freq.
1	50937.630	2.367 ± 0.067	0.764 ± 0.014	19.03 ± 0.380	10.05 ± 0.100	0.654 ± 0.014	3.000 ± 0.200	-	-
2	50939.070	2.356 ± 0.052	0.738 ± 0.012	18.71 ± 0.374	8.851 ± 0.088	0.678 ± 0.015	3.500 ± 0.200	-	-
3	50942.010	2.422 ± 0.068	0.758 ± 0.011	15.49 ± 0.309	10.24 ± 0.102	0.602 ± 0.013	2.500 ± 0.300	-	-
4	50945.860	2.317 ± 0.092	0.711 ± 0.016	12.70 ± 0.254	6.887 ± 0.068	0.648 ± 0.014	4.000 ± 0.500	-	-
5	50949.740	2.072 ± 0.058	0.601 ± 0.012	10.71 ± 0.214	3.826 ± 0.038	0.736 ± 0.016	2.000 ± 0.800	-	-
6	50951.670	1.916 ± 0.027	0.461 ± 0.017	13.33 ± 0.266	1.201 ± 0.024	0.917 ± 0.022	10.20 ± 0.600	4.235 ± 0.337	3.390 ± 0.008
7	50952.490	1.858 ± 0.032	0.466 ± 0.024	9.092 ± 0.181	0.980 ± 0.029	0.902 ± 0.022	11.30 ± 0.800	3.540 ± 0.247	2.613 ± 0.012
8	50953.490	1.798 ± 0.027	0.487 ± 0.024	10.64 ± 0.212	0.822 ± 0.024	0.928 ± 0.022	13.60 ± 0.700	3.140 ± 0.128	1.351 ± 0.012
9	50956.960	1.793 ± 0.037	0.459 ± 0.026	7.013 ± 0.140	0.510 ± 0.025	0.932 ± 0.023	15.90 ± 1.100	1.187 ± 0.350	0.430 ± 0.006
10	50958.960	1.675 ± 0.031	0.486 ± 0.025	7.442 ± 0.148	0.565 ± 0.028	0.929 ± 0.023	16.10 ± 1.500	0.922 ± 0.197	0.365 ± 0.011
11	50962.960	1.584 ± 0.024	0.452 ± 0.029	8.827 ± 0.176	0.406 ± 0.040	0.956 ± 0.024	17.30 ± 0.800	0.887 ± 0.058	0.228 ± 0.003

TABLE 5
PARAMTERS FOR 4U 1630–47 IN 1999

Obs.	Date	Γ	T_{in}	Power law Fl.	Dbb Fl.	PLR	rms (%)	ν_1	QPO Freq.
1	51388.3	2.060 ± 0.036	0.511 ± 0.014	9.891 ± 0.197	2.414 ± 0.048	0.803 ± 0.019	<2	-	-
2	51389.1	1.987 ± 0.028	0.519 ± 0.011	10.09 ± 0.201	2.274 ± 0.045	0.816 ± 0.019	<2	-	-
3	51390.1	2.036 ± 0.032	0.529 ± 0.014	8.340 ± 0.166	2.140 ± 0.042	0.795 ± 0.019	<2	-	-
4	51391.4	2.014 ± 0.032	0.500 ± 0.016	7.680 ± 0.153	1.557 ± 0.046	0.831 ± 0.020	<2	-	-
5	51393.2	1.834 ± 0.024	0.464 ± 0.014	8.301 ± 0.166	1.220 ± 0.061	0.871 ± 0.022	<2	-	-
6	51394.8	1.845 ± 0.024	0.469 ± 0.027	7.294 ± 0.145	0.796 ± 0.055	0.901 ± 0.023	12.50 ± 2.850	4.090 ± 0.089	1.820 ± 0.004
7	51395.5	1.881 ± 0.031	0.429 ± 0.032	6.033 ± 0.120	0.694 ± 0.062	0.896 ± 0.024	8.553 ± 1.000	0.603 ± 0.517	0.782 ± 0.083
8	51397.2	2.041 ± 0.076	0.424 ± 0.058	3.483 ± 0.104	0.438 ± 0.043	0.888 ± 0.035	<4	-	-
9	51398.2	1.802 ± 0.093	0.378 ± 0.041	3.854 ± 0.154	0.351 ± 0.035	0.916 ± 0.046	<4	-	-
10	51400.1	2.048 ± 0.061	0.425 ± 0.053	2.852 ± 0.142	0.251 ± 0.025	0.919 ± 0.057	<4	-	-

TABLE 6
PARAMTERS FOR 4U 1630–47 IN 2001

Obs.	Date	Γ	T_{in}	Power law Fl.	Dbb Fl.	PLR	rms (%)	ν_1	QPO Freq.
1	52048.0	2.219 ± 0.039	0.784 ± 0.012	18.01 ± 0.360	15.18 ± 0.151	0.542 ± 0.011	<2	-	-
2	52049.8	2.236 ± 0.034	0.702 ± 0.012	15.27 ± 0.305	10.19 ± 0.101	0.599 ± 0.013	<2	-	-
3	52051.6	2.260 ± 0.029	0.674 ± 0.012	14.32 ± 0.286	7.206 ± 0.072	0.665 ± 0.014	<2	-	-
4	52053.8	2.095 ± 0.020	0.592 ± 0.011	13.25 ± 0.265	4.642 ± 0.046	0.740 ± 0.016	<2	-	-
5	52055.6	2.230 ± 0.038	0.542 ± 0.014	9.742 ± 0.194	3.458 ± 0.069	0.738 ± 0.017	<2	-	-
6	52058.0	1.970 ± 0.030	0.460 ± 0.017	10.29 ± 0.205	1.760 ± 0.052	0.853 ± 0.021	<2	-	-
7	52059.4	1.575 ± 0.010	0.401 ± 0.016	11.06 ± 0.221	0.895 ± 0.062	0.925 ± 0.024	11.72 ± 2.730	2.520 ± 1.070	1.396 ± 0.042
8	52061.6	1.683 ± 0.030	0.463 ± 0.023	4.766 ± 0.142	0.767 ± 0.053	0.861 ± 0.033	9.323 ± 3.150	0.297 ± 0.069	-
9	52063.6	1.751 ± 0.026	0.444 ± 0.014	3.961 ± 0.158	0.590 ± 0.047	0.870 ± 0.044	<5	-	-
10	52065.9	1.694 ± 0.021	0.430 ± 0.025	3.880 ± 0.194	0.491 ± 0.049	0.887 ± 0.056	<5	-	-

TABLE 7
PARAMTERS FOR XTE J1748–288

Obs.	Date	Γ	T_{in}	Power law Fl.	Dbb Fl.	PLR	rms (%)	ν_1	QPO Freq.
1	51002.7	2.643 ± 0.031	0.892 ± 0.015	17.73 ± 0.354	9.967 ± 0.099	0.640 ± 0.014	<2	-	-
2	51007.3	1.967 ± 0.017	0.437 ± 0.015	19.62 ± 0.392	2.496 ± 0.074	0.887 ± 0.021	4.250 ± 0.250	-	-
3	51012.2	1.874 ± 0.005	0.396 ± 0.030	10.07 ± 0.201	0.253 ± 0.025	0.975 ± 0.024	21.14 ± 3.160	1.104 ± 0.186	-
4	51024.4	1.828 ± 0.013	0.399 ± 0.019	8.879 ± 0.177	0.270 ± 0.027	0.970 ± 0.024	20.71 ± 0.370	0.220 ± 0.014	-

TABLE 8
PARAMTERS FOR GRO J1655–40

Obs.	Date	Γ	T_{in}	Power law Fl.	Dbb Fl.	PLR	rms (%)	ν_1	QPO Freq.
1	50658.4	2.106 ± 0.029	0.898 ± 0.004	16.25 ± 0.325	57.22 ± 0.572	0.221 ± 0.004	1.800 ± 0.100	-	-
2	50663.7	2.392 ± 0.092	0.795 ± 0.003	9.031 ± 0.180	29.68 ± 0.296	0.233 ± 0.004	<2	-	-
3	50674.4	1.948 ± 0.010	0.610 ± 0.027	27.59 ± 0.551	1.220 ± 0.036	0.957 ± 0.023	22.66 ± 0.770	1.514 ± 0.077	6.457 ± 0.020
4	50678.6	1.670 ± 0.015	0.629 ± 0.077	9.284 ± 0.278	0.203 ± 0.020	0.978 ± 0.036	24.34 ± 2.390	0.313 ± 0.027	0.785 ± 0.011
5	50685.4	1.751 ± 0.057	0.485 ± 0.026	0.971 ± 0.058	0.072 ± 0.007	0.930 ± 0.068	<5	-	-